# Phonon Thermal Conduction in Periodically Porous Silicon Nanobeams

Woosung Park[1], Amy M. Marconnet[2], Takashi Kodama[1], Joonsuk Park[3], Robert Sinclair[3], Mehdi Asheghi[1], and Kenneth E. Goodson[1]
[1]Department of Mechanical Engineering, Stanford University, Stanford, California, United States, 94305
[2]School of Mechanical Engineering, Purdue University, West Lafayette, Indiana, United States, 47907
[3]Department of Materials Science and Engineering, Stanford University, Stanford, California, United States, 94305
Email: parkws@stanford.edu

## ABSTRACT

The thermal conductivity of single crystal silicon can be reduced by the introduction of boundaries at the nanoscale. We present the measured thermal conductivity of single crystal silicon nanobeams patterned with a single row of holes at room temperature: the hole diameter and the spacing vary from 100nm to 250nm and from 200 nm to 800nm, respectively. A steady-state four-probe joule heating measurement technique is used to extract the thermal conductivity of the porous silicon nanobeams across a range of pore geometries. The reduction in thermal conductivity owing to the hole boundaries is up to a factor of two.

**KEY WORDS:** Silicon Porous Nanobeam, Porous Silicon, Thermal Conductivity, Phononic Crystal, Holey Silicon.

## NOMENCLATURE

| | |
|---|---|
| A | Cross section area |
| H | Thickness of layer |
| I | Electrical current |
| $k$ | In-plane thermal conductivity |
| L | Length of the sample |
| $L_0$ | Lorentz Constant |
| R | Electrical Resistance |
| W | Width of the sample |

### Greek Symbol

| | |
|---|---|
| $\alpha$ | Temperature coefficient of resistance |
| $\rho$ | Electrical resistivity |
| $\sigma$ | Electrical conductivity |

### Subscripts

| | |
|---|---|
| Si | Silicon layer |
| Pd | Palladium metal layer |
| eff | Effective property |
| 0 | Joule heating free state |

## Introduction

The thermal conductivity of single crystal silicon can be reduced by the introduction of boundaries at the nanoscale [1-4]. Recent work on silicon films and nanobeams patterned with periodic arrays of nanoscale cylindrical holes has shown that the thermal conductivities of the films may be reduced in a manner that differs from the predictions of classical phonon transport theory [3, 4]. More work is required to determine if the periodic pore structure may influence phonon dispersion, or whether coherence effects may influence boundary scattering physics. Thermal transport in 2D periodically porous films, which are sometimes referred to as phononic crystals, has recently been studied across a range of pore geometries [3, 5, 6].

This work continues our focus on silicon nanobeams patterned with a single row of holes, which provides an interesting approach to studying the interplay of heat diffusion, boundary scattering, and coherence. Here we report thermal conductivity of silicon nanobeams with different hole diameters and spacing at room temperature. An improved steady-state four-probe joule heating measurement technique is used to extract the thermal conductivity of the porous silicon nanobeams across a range of pore geometries.

### Sample Fabrication & Measurement

Porous nanobeam samples are fabricated with variations in two controlled parameters: cylindrical hole diameters (D) and hole spacing (S). First, the single crystal silicon device layer of a silicon on-insulator (SOI) wafer is reduced to 198nm thick using thermal oxidation and wet etching. Then, all structures, including the beam, nanoscale holes, and electrical contact pads, are patterned using electron beam lithothography to achieve nanoscale feature sizes. The patterned silicon is then etched anisotropically, and the structures are suspended using a wet etch process. Finally, a silicon dioxide is deposited using Plasma Enhanced Chemical Vapor Deposition (PECVD) as an electrical passivation layer, followed by 40nm of palladium metal, which is deposited on top of the oxide using an electron beam evaporator. This serves as the heater and thermometer for the joule heating measurement.

The fabricated dimensions of the samples are determined from the Scanning Electron Microscope (SEM) and Transmission Electron Microscopy (TEM) images shown in Figure 1, which depicts the densest and largest pore structure. In this work, we control two parameters: hole diameter and the spacing; all other dimensions remain constant for all samples. The length (L=19.35μm) of the sample is determined using

Table 1. Sample Dimensions

| Sample | 1 | 2 | 3 | 4 | 5 |
|---|---|---|---|---|---|
| Diameter (nm) | 100±15 | 100±15 | 100±15 | 260±15 | 260±15 |
| Spacing (nm) | 200±10 | 300±10 | 400±10 | 400±10 | 600±15 |

5000x magnification SEM images, and hole diameter (D), spacing (S), and width (W) are calculated from the 10000x magnification SEM images, shown in Figure 1 (a) and (b) respectively. The thick and bright boundary of the sample causes uncertainty in determination of the sample dimensions. This uncertainty is inherent to SEM and is caused by scattered electrons at the edge. The boundary corresponds to the sidewall of the nanobeam shown in Figure 1 (c), and the slope is caused by differences in the dry etching exposure time

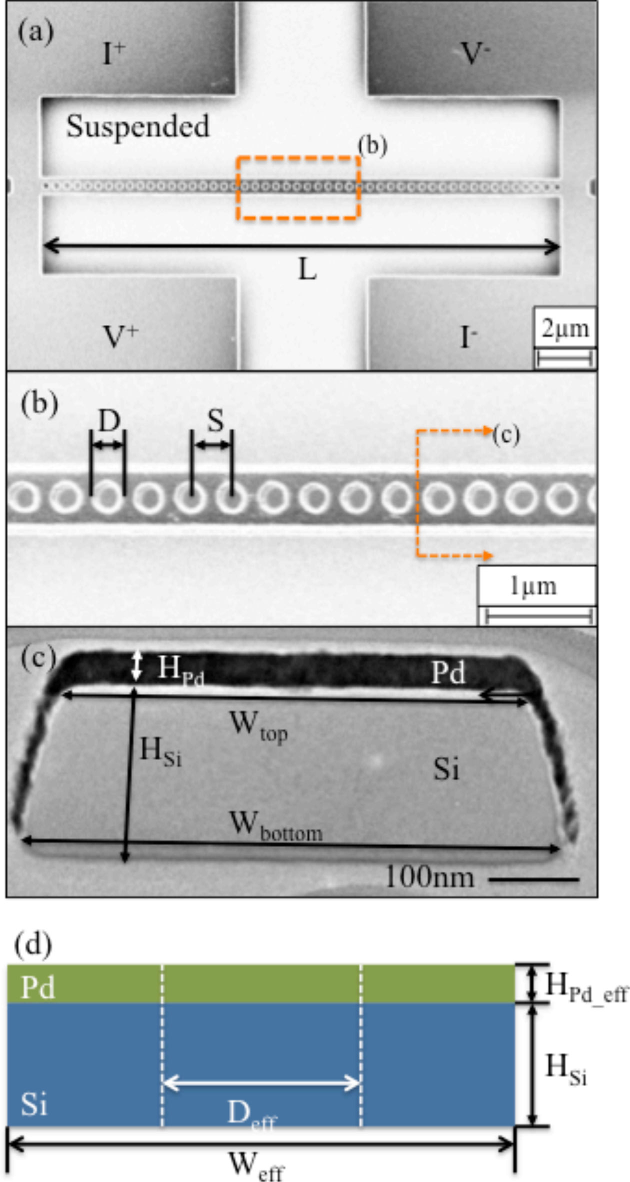


**Figure 1. Structural characterization of porous silicon nanobeam.** (a) Top view of sample 5 with 5000x magnification SEM, where L is 19.35μm, (b) Close-up top view of sample 5 with 10000x magnification SEM, where S is 400nm, (c) Cross-section of sample 5, $W_{top}$(560nm) and $W_{bottom}$ (680nm) match with inner and outer boundaries of the beam respectively, $H_{Si}$ and $H_{Pd}$ are 198nm and 38nm respectively, (d) Schematic geometry for sample 5 that is used in the analysis; $W_{eff}$, $D_{eff}$, and $H_{Pd_eff}$ are 620nm, 260nm, and 51nm.

between the top and the bottom surfaces. In this work, we assume that the samples have perfectly rectangular cross-sections to reduce computing cost for analysis, as shown in Figure 1 (d). The assumed rectangular boundaries are taken to be the average values of the inner and outer edges of the thick boundary lines and are then used to calculate the effective width ($W_{eff}$) and hole diameters ($D_{eff}$). Additionally, the effective thickness of the metal layer used in the analysis is chosen such that the product of the effective width and thickness is equal to the actual area measured by TEM, as shown in Figure 1(c). According to a 3D COMSOL simulation, the difference in the extracted thermal conductivity using the actual trapezoidal structure and the rectangular simplification causes less than 1% deviation from the true thermal conductivity for the most complicated sample structure at room temperature. The details of these sample geometries are described in Table 1.

We characterize the thermal conductivity of the samples using a four-probe, steady-state electro-thermal measurement technique [4, 7], with all samples measured under vacuum conditions below $2\times10^{-3}$ Torr to minimize convection effects. A DC electrical current conducts through the palladium metal film. This causes joule heating and a subsequent temperature rise in the metal film, which is measured by the change in the resistance. The temperature profile and corresponding resistance are calculated analytically for the non-porous reference sample (Eq. (1,2) respectively), assuming 1D conduction and constant material properties [4]:

$$T(x) = T_0 - \frac{1}{\alpha}\left(1 - \frac{\cos\gamma x}{\cos\left(\frac{\gamma L}{2}\right)}\right) \text{ and} \quad (1)$$

$$R = R_0\left(\frac{2}{\gamma L}\tan\left(\frac{\gamma L}{2}\right)\right), \quad (2)$$

where $\gamma = \sqrt{\frac{I^2 R_0 \alpha}{WL(k_{Pd}H_{Pd\,eff}+k_{Si}H_{Si})}}$, $A_{Pd} = H_{Pd\,eff}W(x)$, $\rho(T) = \rho_0(1+\alpha(T-T_0))$, $A_{Si} = H_{Si}W(x)$. For the porous samples, the temperature profile and corresponding resistance are calculated numerically by discretizing the heat diffusion equation accounting for the variation in the cross-sectional area for heat transport. The 1D conduction assumption has a maximum of 6% deviation in thermal conductivity when compared to a 3D COMSOL simulation. The electrical resistance of the metal layer is calculated for the applied current with the above equations, and the thermal conductivity of the silicon nanobeam is determined by fitting the measured electrical resistance with the computed value. Three parameters of the metal must be determined before fitting for the thermal conductivity of the nanobeam: electrical conductivity, temperature coefficient of resistance (TCR), and thermal conductivity. The electrical conductivity of the metal is extracted numerically from the electrical resistance measurement performed in the small joule heating region shown in Figure 2 (a), where the temperature rise due to joule heating can be neglected. Temperature-controlled electrical resistance measurements in this regime provide the TCR of the metal, and its profile is seen in Figure 2 (b). The thermal conductivity of the metal layer is determined using the Weidman Franz Law, $k/\sigma = L_0 T$, where $k$ is thermal

conductivity, $\rho$ is electrical conductivity, and $L_0$ is the Lorentz number. The Lorentz constant of the metal layer is measured after etching away the silicon layer of the reference sample, and the value is determined to be $(2.44 \pm 2.5)\times10^{-8}$ from 290 to 325K. The measured Lorentz constant is used for the porous silicon nanobeam as well, because the electron mean free path is much smaller than the feature size. The thermal conductivity profile of the metal layer shown in Figure 2 (b) lies in a reasonable range, as determined by temperature-dependent thermal conductivity values of platinum films on the same order of thickness [8]. Although the thermal conductivities of the metal layers may have been underestimated due to neglecting the phonon contribution to thermal transport in the metal, this uncertainty is within the acceptable range. The thermal transport through the metal layer is reasonably small as its thickness is less than 20% of that of the silicon layer.

**Result & Discussion**

Figure 3 shows the measured thermal conductivities for the silicon nanobeams with different hole diameters at room temperature. When compared to the thermal conductivity of the reference non-porous silicon nanobeam, there are two important results: 1) Introduction of holes into the silicon nanobeams leads to a dramatic reduction in the thermal conductivities of the nanobeams. Though the presence of holes increases phonon-boundary scattering as discussed in a previous study, the amount of reduction in thermal conductivity observed in this work is much larger than the reduction of thermal conductivities reported in the previous literature[5]. Thus, we may need to consider other phonon transport reduction mechanisms. 2) More interestingly, the thermal conductivities of porous structures have weaker dependence on spacing than on the hole diameter as shown in the inset of Figure 3. This indicates that the increased boundary scattering between holes owing to the introduction of holes is not critical in phonon thermal transport as the length scale of the holes and the spacing is in the ballistic phonon transport regime. [9]

The measured thermal conductivity for the nanobeam with 260nm hole diameter in this work is an order of magnitude larger than those reported by Marconnet *et al*. [4]. The sample used in their study [4] consisted of a middle porous section and non-porous parts at both ends. The thermal conductivity value of the porous region was extracted assuming thermal conductivity of thin silicon film for the nonporous section, resulting in extraordinary small value in the thermal conductivity for the porous portion of the silicon beam. This approach implies that the porous portion of the beam has very little or no impact on the phonon spectrum and transport within the nonporous section of the beam. This also brings to the forefront a necessary discussion on how to extract the thermal conductivity value for 2D porous arrays and 1D nanoladders for the structures that have sparse holes. It is not clear if the extracted thermal conductivity using the Fourier's heat conduction would reflect the physics of the problem that contains regions where both diffusion and ballistic heat transfer prevail. In another word, if the holes are sparse and located several mean free paths apart, then one may consider piecewise heat conduction analysis that includes both diffusion and ballistic regimes, but this may result in some inconsistencies. If the holes are spaced within (or smaller

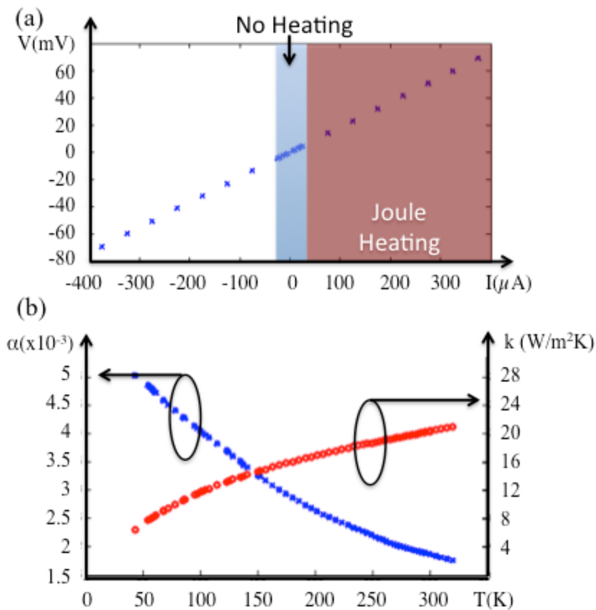


**Figure 2. Electrical measurement and thin palladium metal layer electro and thermal properties.** (a) IV sweep per temperature point. ~~No~~ temperature rise is assumed in the no heating region (<30μA) due to lack of joule heating. This region is used to determine the electrical and thermal conductivities and TCR of the metal layer. Data points in the joule heating region (30μA ~ 300μA) are used for data fitting. (b) Blue and red color profiles indicate TCR and thermal conductivity of the metal layer for the reference sample.

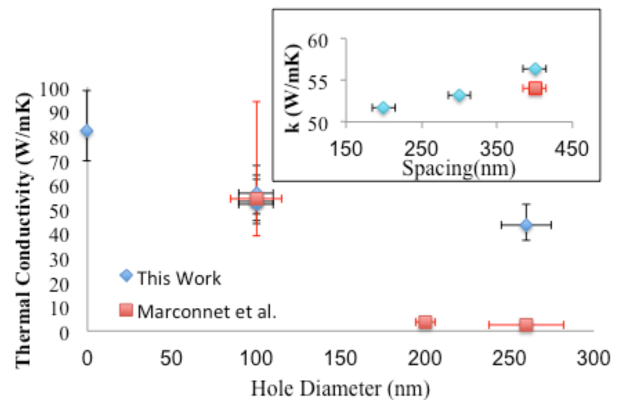


**Figure 3: Room temperature porous silicon nanobeam thermal conductivity.** The blue dots refer to the experimentally measured thermal conductivity of the silicon porous nanobeam. Each dot has 19% uncertainty in thermal conductivity and up to 15% uncertainty in hole diameter. Measured absolute temperature variation is 295±3K. Thermal conductivities for 100nm hole diameter nanobeams with spacings 200, 300, and 400 nm are shown in the inset. Red dots denote the thermal conductivity value for porous silicon nanobeam that Marconnet *et al.* report.

than) one mean free path of the phonons -- and the structure is homogeneous, then one may consider reporting a “representative” thermal conductivity value.

Uncertainty in the sample dimensions is the dominant source of error in the analysis because the thermal transport capability of the structure is strongly related to the cross-section of the sample. Though a TEM image improves the measurements, the inherent pixellation of the image introduces an error in the extracted thermal conductivity of the order of 10%. An additional 6% error is introduced by the 1D conduction assumption, since the pores in the nanobeam cause the isotherms to bend. We also note that the error resulting from an uncertainty in the thermal conductivity of the metal is insignificant because the thin metal layers have a much higher thermal resistance than the thick silicon beam. The silicon dioxide passivation layer has a large thermal resistance, forcing conduction through the other heat path (e.g. the silicon and the metal). Finally, the thermal boundary resistance between layers is ignored in this steady-state measurement.

**Conclusion**

In summary, we measured the thermal conductivity for single crystal silicon porous nanobeams with various hole diameters, from 100nm to 260 nm, and spacing from 200 to 400nm. Two important features of this work are: 1) the thermal conductivity for nanobeams with holes is significantly lower than the non-porous reference, and 2) thermal conductivity depends rather weakly on the hole spacing, indicating unknown phonon behavior besides introduced boundary scattering. Future work, including temperature dependent measurements, will further explore these phonon transport mechanisms.

**Acknowledgements**

The authors acknowledge the support of the Semiconductor Research Corporation under Task ID 2308.002 and the National Science Foundation under Award No. 13336734.

**References**

[1] J. Tang, H.-T. Wang, D. H. Lee, M. Fardy, Z. Huo, T. P. Russell*, et al.*, "Holey silicon as an efficient thermoelectric material," *Nano letters,* vol. 10, pp. 4279-4283, 2010.

[2] D. Song and G. Chen, "Thermal conductivity of periodic microporous silicon films," *Applied physics letters,* vol. 84, pp. 687-689, 2004.

[3] P. E. Hopkins, C. M. Reinke, M. F. Su, R. H. Olsson, E. A. Shaner, Z. C. Leseman*, et al.*, "Reduction in the Thermal Conductivity of Single Crystalline Silicon by Phononic Crystal Patterning," *Nano Letters,* vol. 11, pp. 107-112, 2011/01/12 2010.

[4] A. M. Marconnet, T. Kodama, M. Asheghi, and K. E. Goodson, "Phonon Conduction in Periodically Porous Silicon Nanobridges," *Nanoscale and Microscale Thermophysical Engineering,* vol. 16, pp. 199-219, 2012.

[5] Bongsang Kim, Janet Nguyen, Peggy J. Clews, Charles M. Reinke, Drew Goettler, Zayd C. Leseman*, et al.*, "Thermal conductivity manipulation in single crystal silicon via lithographically defined phononic crystals," *Micro Electro Mechanical Systems (MEMS), 2012 IEEE 25th International Conference on,* 2012.

[6] J.-K. Yu, S. Mitrovic, D. Tham, J. Varghese, and J. R. Heath, "Reduction of thermal conductivity in phononic nanomesh structures," *Nat Nano,* vol. 5, pp. 718-721, 10//print 2010.

[7] W. Liu and M. Asheghi, "Thermal conductivity measurements of ultra-thin single crystal silicon layers," *Journal of heat transfer,* vol. 128, pp. 75-83, 2006.

[8] S. Yoneoka, J. Lee, M. Liger, G. Yama, T. Kodama, M. Gunji*, et al.*, "Electrical and thermal conduction in atomic layer deposition nanobridges down to 7 nm thickness," *Nano letters,* vol. 12, pp. 683-686, 2012.

[9] J.-P. M. Péraud and N. G. Hadjiconstantinou, "Efficient simulation of multidimensional phonon transport using energy-based variance-reduced Monte Carlo formulations," *Physical Review B,* vol. 84, p. 205331, 11/21/ 2011.